

# The Identification of Explosives in Millimeter-Wave Imaging Systems

James C. Weatherall<sup>a</sup>, Jeffrey Barber<sup>b</sup>, Kevin Yam<sup>a</sup>, Peter R. Smith<sup>c</sup>, Joseph Greca<sup>a</sup>, and Barry T. Smith<sup>b</sup>

<sup>a</sup>Battelle, Bldg. 315, FAA Technical Center, Atlantic City NJ 08405, USA

<sup>b</sup>Transportation Security Laboratory, U.S. Department of Homeland Security, Bldg. 315, FAA Technical Center, Atlantic City NJ 08405, USA

<sup>c</sup>AASKI, Inc., Bldg. 315, FAA Technical Center, Atlantic City NJ 08405, USA

## ABSTRACT

Commercial Advanced Imaging Technology (AIT) systems use arrays or synthetic arrays of millimeter wave antennas to generate holographic images and identify anomalies in those images that may present threats. In order to provide additional information for the AIT assessment, we are developing a technique that enables the identification of threat composition based on dielectric constant. The dielectric constant is extracted from the spectral content of the broadband holographic imaging data. The technique is demonstrated from images collected in a prototype personnel-screening system. The dielectric constant is obtained by numerically fitting the reflection coefficient as a function of frequency to an optical model. The reflection coefficient is a function of frequency because of propagation effects, such as multiple reflections and energy loss, that are associated with the material's complex dielectric constant. In order to accomplish the analysis using an imaging system, the spectrum is obtained from an integration of the reflectivity image spectrum, which is an intermediate result in the image reconstruction algorithm. The present use of an imaging array demonstrates the ability to detect dielectric constant in small areas on a complex target. In principle, the implementation of this technique in standoff imaging systems would allow threat assessment to be accomplished within the scope of millimeter-wave screening.

**Keywords:** Millimeter-wave imaging, parameter extraction, dielectric measurement, reflection coefficient, detection algorithm, explosive detection, advanced imaging technology, AIT

## 1. INTRODUCTION

Millimeter-wave imaging is used in Advanced Imaging Technology (AIT) for passenger screening. As currently implemented, image anomalies posing potential threats are determined using Automatic Target Recognition (ATR) algorithms and projected onto a featureless generic outline of a person<sup>1</sup> without identifying material properties of the threat. Commercial examples of millimeter-wave imaging systems are the L3 Provision and the Rohde & Schwarz QPS200. In addition, the Pacific Northwest National Laboratory (PNNL) has developed a high definition (HD) prototype imaging system which is being used for experimental development at the Transportation Security Laboratory (TSL), which is part of the U.S. Department of Homeland Security, Science and Technology Directorate. The PNNL HD AIT system broadly updates the design described in Ref. 2, and performs 3D imaging using a broadband of millimeterwaves.

The underlying images used for AIT are holographic reconstructions generated from a broadband of frequencies. In recent work, we have proposed using the frequency content of the image to infer the index of refraction of the target anomaly.<sup>3-6</sup> The index of refraction,  $n$ , is related simply to the relative dielectric constant,  $\epsilon$ , such that  $\epsilon = n^2$  for nonmagnetic materials. Note that the dielectric constant is a complex quantity, where the real part describes polarization and propagation properties, and the imaginary part the dielectric loss. The dielectric constant can be applied as discriminatory data on the target composition, and can potentially identify explosive

---

Further author information: Send correspondence to J.C.W., E-mail: james.weatherall@associates.hq.dhs.gov

threats during the screening process. This work has progressed from first demonstrating how the free-space millimeter-wave reflectivity spectrum can detect dielectric constant,<sup>5</sup> to making use of the reflectivity data from a scanning array to accomplish the dielectric detection.<sup>6</sup> In this work, we use an imaging system to accomplish the dielectric detection.

## 2. EXPERIMENTAL APPROACH

The PNNL HD imaging system collects quasi-monostatic radar data, sampling uniformly at sub-wavelength scale over the full cylindrical area enclosing the screening volume. The technique uses electronic switching in a linear antenna column that mechanically scans across the cylindrical aperture.<sup>7,8</sup> The system records the reflection in-phase and quadrature (IQ) data for each array element at 512 frequencies across the 10 – 40 GHz band. From this data, a holographic imaging algorithm can be applied to construct a reflectivity image of the target. In processing the data for imaging, the frequency content is incorporated into the image construction to achieve the spatial resolution.<sup>2</sup> An alternate approach, which we describe in more detail below, is to use the frequency content to acquire a reflection spectrum of limited areas on the image.

Figure 1(a) shows the integrated reflection amplitude for a finite area on the cylindrical aperture. The target in this example is 1.7 cm of paper stacked on a 30 × 30 cm metal plate held by a person. A small, thin 10 × 10 cm metal plate is attached at the top of the target, above the stack. Although the IQ projection is unfocused, because of specular reflection the structure of the target is still apparent. The reconstructed target is shown in Fig. 1(b). The spectrum-image, which is extracted from an intermediate stage of the reconstruction (see Sec. 4), is shown at a fixed-frequency in Fig. 1(c). The effect of the array aperture is to resolve the specular reflection into a small angular range normal to the flat surface of the target.

A calibration is applied to the reflectivity data in order to adjust the phase to a reference plane at the target surface, and to normalize amplitude to unity for a perfect reflector. This enables the use of the IQ components of the reflectivity in the dielectric analysis. While calibration techniques to derive the reflectivity from reflection data for a single antenna are known,<sup>9,10</sup> they have not – to our knowledge – been used for imaging arrays. Our use of the imaging array for dielectric metrology is thus unique. For our application, a one port systemic error model, similar to that used in network analyzers, is applied for PNNL data error correction. The result is shown in Fig. 2 for a spectrum from a 30 × 30 × 2.54 cm polymethyl methacrylate (PMMA) sheet backed with metal, and corrected using the one port model and time-gated around the range of interest. The calibration standards are verified to have the correct response. The short, i.e. a metal plate at the reference plane, shows a correct reflectivity of -1 over the frequency range. Similarly, the absorbing RAM material is zero over the frequency

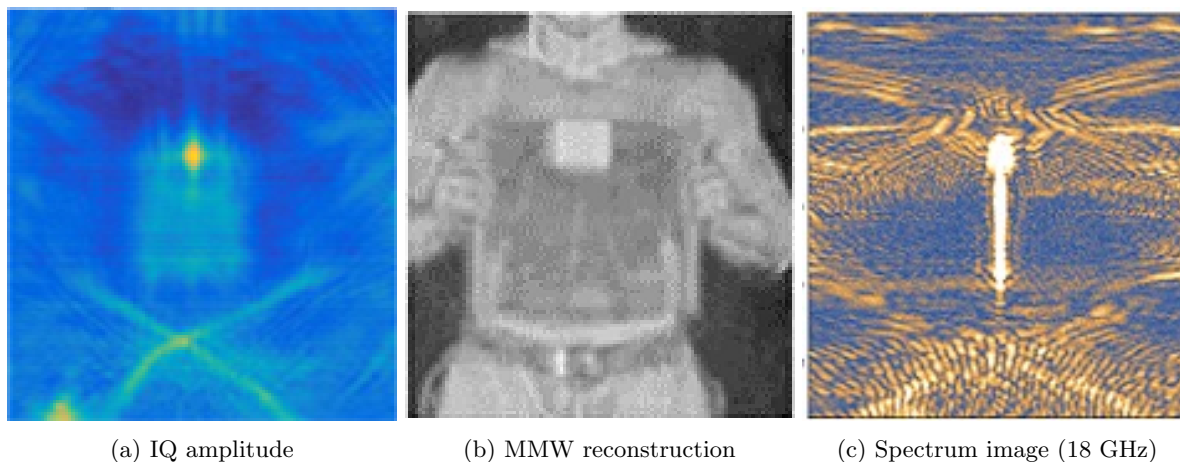


Figure 1: Images of paper stack.

range, and the offset short, which displaces the metal 1/4 wavelength at band center, has unit reflectivity and the appropriate phase variation over the frequency range. The corrected PMMA spectrum in Fig. 2 exhibits the classical interference effects important for our dielectric measurement. The quality of corrected and gated data illustrates the abundant dynamic range in the PNNL data.

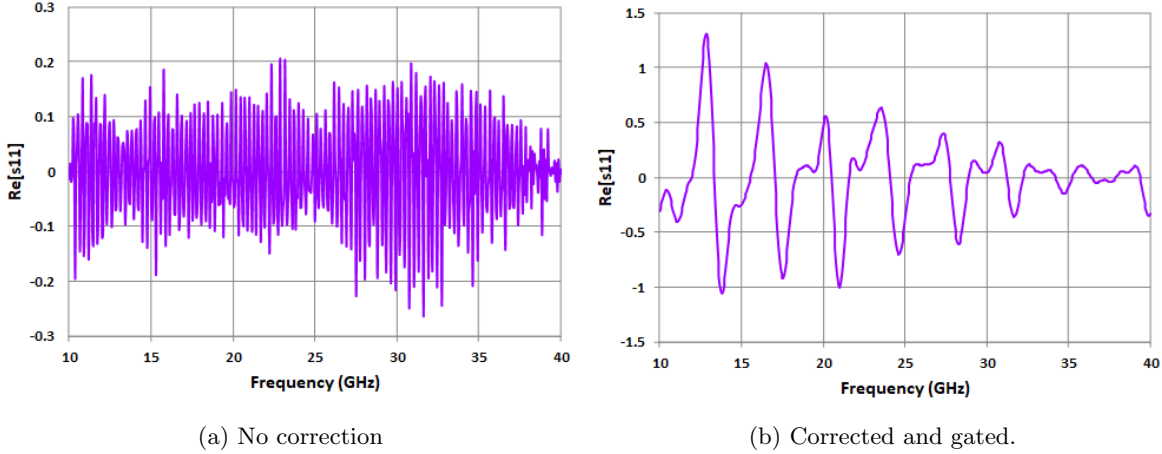


Figure 2: The in-phase components for the PMMA target.

### 3. DETECTION METHODOLOGY

As carried on the body, explosives are materials layered against a reflective surface. Because of transmission through the material, the reflection from the front surface and back surface (and multiple internal reflections) can interfere constructively or destructively, depending on frequency. The reflection and transmission coefficients depend on the refractive index, so the total reflection spectrum is a function of dielectric constant, as well as the thickness of the material. The free parameters – real component of the index, imaginary component, and thickness – are derived from the data by fitting to a reflectivity model, as described below.

The reflectivity model is based on the Fresnel equations, which describe optical reflection and transmission through interfaces of materials with different refractive index.<sup>11,12</sup> We consider a system with two interfaces with three components of refractive index  $n_0$ ,  $n_1$ , and  $n_2$ , corresponding to air, the target, and the background, respectively. Reflection and transmission coefficients are defined as ratios of the respective electric fields relative to the incident electric field, inclusive of phase. The angle of incidence is assumed normal to the surface because the system is quasi-monostatic, and generally the target presents a surface facing the transmitter array. The reflection and transmission coefficients for fields propagating from 0 to 1 are  $r_1$  and  $t_1$ ; the reflection coefficient at the interface 1 to 2 is  $r_2$ ; and, the reflection and transmission coefficients for fields propagating outward from 1 to 0 are  $r'_1$  and  $t_0$ .

The total of the reflected electric field includes all the reflections on the front and back surface, and multiple internal reflections escaping the slab. The sum of the fields, normalized to the incident field to give the reflection coefficient, is written

$$r = r_1 e^{i\theta_0} + t_0 r_2 t_1 (e^{i\theta_1} + (r'_1 r_2) e^{i\theta_2} + (r'_1 r_2)^2 e^{i\theta_3} + \dots), \quad (1)$$

where  $\theta_m$  represents the phase incremented by the propagation. The phasing constant for  $m$ -propagations to-and-from the front and back surface separated by a thickness  $\Delta L$  is  $\theta_m = \theta_0 + m n_1 (2\pi f/c) (2\Delta L)$ . The imaginary component of  $n_1$  in the phase term accounts for absorption. Equation 1 is often simplified by summation formula for an infinite geometric series.<sup>12,13</sup> Because perfectly planar surfaces are an idealization, and the fact that repeated internal reflections decrease rapidly in amplitude for semi-transparent materials, we choose a truncated sum, usually with five or fewer terms. The overall phase is  $\theta_0 = 0$  when the calibration puts the reference plane at the front surface.

#### 4. REFLECTIVITY SPECTRUM

The image data consists of a data set of spatial reflectivity measured by antenna array elements located at  $(\omega, \theta, z)$  in a cylindrical column of radius  $R$ . The reflected signal  $r$  measured from a target is a coherent sum at the antenna of the reflection from each point  $(x', y', z')$  in the image space:<sup>14,15</sup>

$$r(\omega, \theta, z) = P(\omega) \int \int \int f(x', y', z') e^{i2k\sqrt{(x'-R\cos\theta)^2+(y'-R\sin\theta)^2+(z'-z)^2}} dx' dy' dz', \quad (2)$$

where  $k = \omega/c$ . The exponential is the phase, advanced for propagation from the antenna to the target point and back to the antenna.

The integral in Eq. 2 is a Green's function representation of the radiation field, absent the  $1/r$  dependence.<sup>15</sup> With the Green's function

$$g_\theta(\omega, x', y', z') = e^{-i2k\sqrt{(x'-R\cos\theta)^2+(y'-R\sin\theta)^2+(z'-z)^2}}, \quad (3)$$

the integral is

$$r(\omega, \theta, z) = P(\omega) \int \int \int f(x', y', z') g_\theta^*(\omega, x', y', z') dx' dy' dz'. \quad (4)$$

A generalized Parseval's theorem is used to write Eq. 4 in the wavenumber domain as follows:

$$r(\omega, \theta, z) = \int \int \hat{f}(k_x, k_y, z') \hat{g}_\theta^*(\omega, k_x, k_y, z') dk_x dk_y dz', \quad (5)$$

where the  $z$ -integration (vertical axis) remains in coordinate space. The hat on  $\hat{f}$  and  $\hat{g}$  denotes a double Fourier transform in  $x$  and  $y$ . Now, we adopt polar coordinates  $(\rho, \phi)$ , where  $k_\rho$  is the magnitude of the spatial wavenumber,  $k_\rho = \sqrt{k_x^2 + k_y^2}$ , and  $\phi$  is the angle  $k_y/k_x = \tan \phi$ . In the polar coordinates,  $dk_x dk_y = k_\rho dk_\rho d\phi$ , and  $k_x \cos\theta + k_y \sin\theta = k_\rho \cos(\theta - \phi)$ . The reconstructed image  $\hat{f}(k_\rho, \phi, z')$  is seen as the basis for extracting the spectrum. Inserting the Green's function into the reflection integral (cf. p. 497, Ref. 15), the spectrum is:

$$r(\omega, \theta, z) = \int_{k_\rho} e^{i\sqrt{4k^2 - k_\rho^2} z} \int_\phi \int_{z'} \hat{f}(k_\rho, \phi, z') e^{-i\sqrt{4k^2 - k_\rho^2} z'} e^{ik_\rho R \cos(\theta - \phi)} dz' d\phi k_\rho dk_\rho. \quad (6)$$

To express the integral in a closed form, we select a ray path at angle  $\theta$  and height  $z$  that corresponds to a specular reflection, and idealize the reflection image as isotropic in angle. In effect, this expands the local reflection into a cylindrically uniform target. With this idealization, the reflection image becomes  $\hat{f}(k_\rho, \phi, z') \rightarrow \hat{f}(k_\rho, \theta, z)$  and is partially extracted from the integral:

$$r(\omega, \theta, z) = \int_{k_\rho} \hat{f}(k_\rho, \theta, z) \int_\phi \int_{z'} e^{i\sqrt{4k^2 - k_\rho^2} (z' - z)} e^{ik_\rho R \cos(\theta - \phi)} dz' d\phi k_\rho dk_\rho. \quad (7)$$

After doing the integrations over  $dz'$  and  $d\phi$ , the remaining integral over  $k_\rho$  represents a decomposition of the isotropic reflection into plane wave components, such that  $k_\rho \rightarrow 2k$ . In this form, the reflectivity spectrum becomes

$$r(\omega, \theta, z) = \hat{f}(k_\rho, \theta, z) k_\rho J_0(k_\rho R). \quad (8)$$

Equation 8 has the form of an plane wave expansion of cylindrical waves. The result illustrates that the underlying spectrum of the target, excluding the effect of geometry, is the function  $\hat{f}(k_\rho, \theta, z)$ .

## 5. RESULTS

For the case of large, flat targets, this analysis produces consistent spectra and good fitting solutions. For example, for a pixel on the spectrum-image of the paper stack on metal background described in Sec. 2, the spectrum and the numerical fitting from the Fresnel model is plotted in Fig. 3. The solution to the dielectric fitting parameters for this PNNL HD image spectrum is  $\epsilon = 2.21 + 0.16i$ ; this compares with the single horn, free-space measurement for paper derived with a more standard calibration and measurement,<sup>3</sup>  $\epsilon = 2.34 + 0.18i$ . The significance of this result is that the spectrum in Fig. 3 has been obtained with the unusual instrumentation of a high resolution imaging array at a distance.

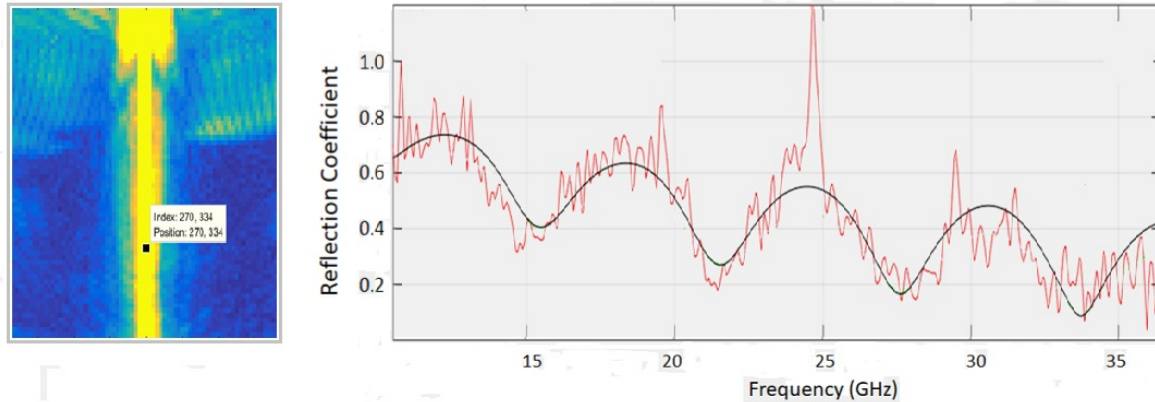


Figure 3: The point on the spectrum-image (left) has the spectrum in the graph. The curve is the numerical fit.

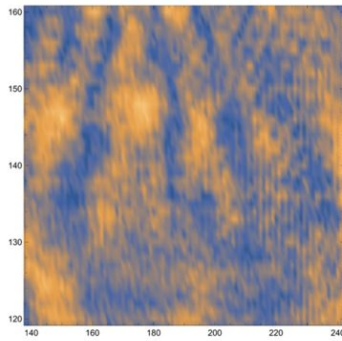
We also show some results for two non-ideal targets, P1000 explosive and a bound paper book, carried on the person. P1000 is Primasheet 1000, a flexible PETN-based explosive sheet;<sup>16</sup> the paper book target is an engineering journal monthly. Figures 4(a)-(b) and 4(c)-(d) show the image of each target at a fixed frequency, and the spectrum extracted from the target. In both cases, the objects are pressed against the body by the person holding the targets. The spectra show similar interference effects against the body as against the metal background, but when the targets lack exact planarity, spatial fringing in the images becomes apparent, and the spectra are more variable, point-to-point. For the back surface in the Fresnel-fitting model, a fixed reflectivity  $r_2 = 0.33$  was used, consistent with the lower range of skin dielectric.<sup>17</sup> The plotted solutions are  $\epsilon = 1.94 + 0.37i$  and  $\epsilon = 2.69 + 0.71i$  for explosive, and book, respectively. The variances in the dielectric detection across the target are large, approximately  $\pm 0.5$  in the real part, and  $\pm 0.1$  in the imaginary part.

## 6. SUMMARY

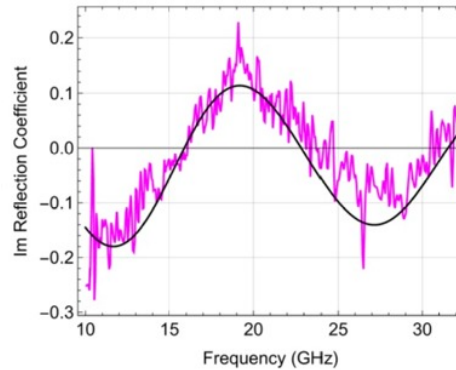
The information in millimeter-wave images provided by reflectivity alone is not specific to the material composition, because the transparency of the material and the net reflectivity varies with thickness. The technique described here uses the spectral information to infer the index of refraction (and dielectric constant of the material) independently from thickness, and this information is applicable to discriminating composition.

This work employs a millimeter-wave imaging system to acquire the required frequency spectra. This has the advantage of using data that is already being collected by commercial systems. The information is normally processed for range resolution in three-dimensional holographic imaging, but here a partial construction of the image is made in two spatial dimensions and frequency. The other advantage is that the application of an array resolves the spectra on small spatial scales, so the detection can be done at a distance.

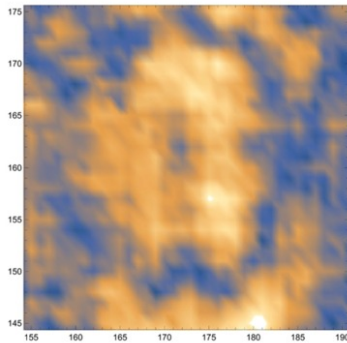
While good dielectric measurement can be achieved off-line with calibration and careful target configuration, more work is needed to apply this technique to targets imaged on people. The challenge is to model the reflectivity in these complex images. Efforts to improve on the consistency of measurement are focusing on statistical analysis, and modification to the reflection model to better represent diffuse reflection and diffraction on small



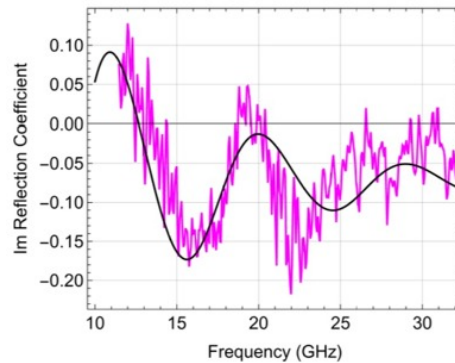
(a) P1000 spectrum-image at 18 GHz



(b) P1000 spectrum and fit



(c) Paper book spectrum-image at 18 GHz.



(d) Paper book spectrum and fit

Figure 4: Dielectric detection of materials from personnel screening images.

targets. Other issues are the effect of target size on the reflectivity normalization, and the characterization of the reflectivity of the back surface of the target against skin.

## ACKNOWLEDGEMENTS

Work was performed under Contract Number HSHQDC-13-A-00023 and DHS Task Order Contract HSHQDC-15-J-00395, Millimeter Wave (MMW) Research and Development. The authors thank K. Babu, DHS S&T HSARPA EXD, for his support.

## REFERENCES

- [1] TSA, "Security Screening." Transportation Security Administration [https://www.tsa.gov/travel/security-screening#quickset-security\\_screening\\_quicktabs\\_4](https://www.tsa.gov/travel/security-screening#quickset-security_screening_quicktabs_4). (Accessed: 6 March 2018).
- [2] Sheen, D. M., McMakin, D. L., Collins, H. D., Hall, T. E., and Severtsen, R. H., "Concealed explosive detection on personnel using a wideband holographic millimeter-wave imaging system," in [*Signal Processing, Sensor Fusion, and Target Recognition V*], *SPIE Proc.* **2755**, 503–514, International Society for Optics and Photonics (1996).
- [3] Weatherall, J. C., Barber, J., and Smith, B. T., "Spectral signatures for identifying explosives with wideband millimeter-wave illumination," *IEEE Transactions on Microwave Theory and Techniques* **64**(3), 999–1005 (2016).

- [4] Weatherall, J. C., Barber, J., and Smith, B. T., “Resonant system and method of determining a dielectric constant of a sample,” (Dec. 12 2017). US Patent 9,841,448.
- [5] Weatherall, J. C., Barber, J., and Smith, B. T., “Identifying explosives by dielectric properties obtained through wide-band millimeter-wave illumination,” in [*Passive and Active Millimeter-Wave Imaging XVIII*], *SPIE Proc.* **9462**, 94620F, International Society for Optics and Photonics (2015).
- [6] Weatherall, J. C., Yam, K., Barber, J., Smith, B. T., Smith, P. R., and Greca, J., “Identifying explosives using broadband millimeter-wave imaging,” in [*Passive and Active Millimeter-Wave Imaging XX*], *SPIE Proc.* **10189**, 1018906, International Society for Optics and Photonics (2017).
- [7] McMakin, D. L., Sheen, D. M., Collins, H. D., Hall, T. E., and Smith, R. R., “Millimeter-wave high-resolution holographic surveillance system,” in [*Substance Detection Systems*], *SPIE Proc.* **2092**, 525–536, International Society for Optics and Photonics (1994).
- [8] Sheen, D. M., McMakin, D. L., and Hall, T. E., “Near field imaging at microwave and millimeter wave frequencies,” in [*Microwave Symposium, 2007. IEEE/MTT-S International*], 1693–1696, IEEE (2007).
- [9] Umari, M. H., Ghodgaonkar, D. K., Varadan, V. V., and Varadan, V. K., “A free-space bistatic calibration technique for the measurement of parallel and perpendicular reflection coefficients of planar samples,” *IEEE Transactions on Instrumentation and Measurement* **40**(1), 19–24 (1991).
- [10] Hock, K. M., “Error correction for diffraction and multiple scattering in free-space microwave measurement of materials,” *IEEE Transactions on Microwave Theory and Techniques* **54**(2), 648–659 (2006).
- [11] Pozar, D. M., [*Microwave Engineering*], New York: John Wiley & Sons (2009).
- [12] Jackson, J. D., [*Classical Electrodynamics*], New York: John Wiley & Sons (1999).
- [13] Bohren, C. F. and Huffman, D. R., [*Absorption and Scattering of Light by Small Particles*], New York: John Wiley & Sons (2008).
- [14] Sheen, D. M., McMakin, D. L., Hall, T. E., and Severtsen, R. H., “Real-time wideband cylindrical holographic surveillance system,” (Jan. 12 1999). US Patent 5,859,609.
- [15] Soumekh, M., [*Synthetic Aperture Radar Signal Processing*], New York: Wiley & Sons (1999).
- [16] Ensign-Bickford Aerospace and Defense Company, “Primasheet 1000 flexible sheet explosive.” EBA&D Product Technical Data Sheet <http://www.eba-d.com/assets/product-sheets/Primasheet-1000-Flexible-Sheet-Explosive-Product-Sheet.pdf>. (Accessed: 14 March 2018).
- [17] Barber, J., Weatherall, J. C., Greca, J., and Smith, B. T., “Toward the development of an image quality tool for active millimeter wave imaging systems,” in [*Passive and Active Millimeter-Wave Imaging XVIII*], *SPIE Proc.* **9462**, 94620D, International Society for Optics and Photonics (2015).